THE ASTROPHYSICAL JOURNAL, 377:171–186, 1991 August 10

WATER IN DENSE MOLECULAR CLOUDS

P. G. WANNIER,[1] L. PAGANI,[2] T. B. H. KUIPER,[1] M. A. FRERKING,[1] S. GULKIS,[1] P. ENCRENAZ,[2,3]
H. M. PICKETT,[1] A. LECACHEUX,[2] AND W. J. WILSON[1]

Received 1990 May 21; accepted 1991 February 8

ABSTRACT

We have used the G.P. Kuiper Airborne Observatory (KAO) to make initial observations of the half-millimeter ground-state transition of water in seven giant molecular clouds and in two late-type stars. No significant detections ($>3\ \sigma$) were made, and the resulting upper limits are significantly below those expected from other, indirect observations and from several theoretical models. The implied interstellar H_2O/CO abundance is less than 0.003 ($3\ \sigma$) in the cores of three giant molecular clouds. This value is less than expected from cloud chemistry models and also than estimates based on HDO and H_3O^+ observations. The limits are derived on the basis of a radiative transfer model incorporating LVG analysis for the low-opacity cloud exterior. Possible explanations for the low implied interstellar H_2O abundance are (1) that fragmentation in dense clouds may cause unexpectedly large levels of ionizing UV radiation, (2) that water may be effectively frozen onto grains, or (3) that the cloud exterior effectively diffuses the emergent radiation.

Subject headings: interstellar: abundances — interstellar: molecules

1. INTRODUCTION

Water may be a particularly important molecule in the interstellar medium (ISM), in part because it may be a major coolant of molecular gas and in part because it may represent a major repository of interstellar oxygen. In addition, oxygen has a cosmic abundance equal, by number, to all other heavy elements combined, making its chemical behavior a vital concern to the understanding of the interstellar medium. One of the major oxygen-bearing interstellar species is thought to be H_2O. The expected range of H_2O/CO in dense clouds with normal, cosmic abundances is between 0.1 and 0.0006, the smallest value pertaining to a metal-deficient gas (Mitchell, Ginsburg, & Kuntz 1978; Prasad & Huntress 1980; Graedel, Langer, & Frerking 1982; Leung, Herbst, & Huebner 1984; Herbst & Leung 1986; Viala 1986; Brown & Rice 1986). Smaller water abundances may apply in carbon-rich ($C/O \geq 1$) regions or in gas exposed to intense ultraviolet (UV) radiation (Herbst & Klemperer 1973). In interstellar clouds which have experienced recent shock waves, theoretical models indicate very large water abundances, approaching that of CO (Iglesias & Silk 1978; Hartquist, Oppenheimer, & Dalgarno 1980; Graff & Dalgarno 1987).

Water has strong transitions throughout the submillimeter and far-infrared wavelength band, but most are blocked by telluric water. The observational basis to date for determining the interstellar water abundance is limited, consisting primarily of a few radio transitions which are superthermally excited. Aside from the 22 GHz water maser line, the most frequently observed radiofrequency line is the 183 GHz 3_{13}–2_{20} transition of $H_2{}^{16}O$, not expected to be thermally excited even in warm (100 K), dense ($10^5\ cm^{-3}$) clouds. It was detected in OMC-1 by Waters et al. (1980) where it was subsequently shown to be radiatively excited and time variable by Kuiper et al. (1984, hereafter KK). The nonthermal nature of the line has been recently confirmed by Cernicharo et al. (1990), who have reported 183 GHz maser emission in several sources, including Orion A. Maser emission is also seen from the 380 GHz (4_{14}–3_{21}) transition toward Orion A likewise adding little information about the actual water abundance (Phillips, Kwan, & Huggins 1980). The 3_{13}–2_{20} transition of $H_2{}^{18}O$ at 203 GHz was reportedly detected in OMC-1 and in DR 21 (Phillips et al. 1978), but these observations may have been confused with high-velocity emission from a nearby line of SO_2 (Erickson & Plambeck 1987). Recently, this situation has been clarified by more detailed observations and the 203 GHz $H_2{}^{18}O$ line has been identified (Jacq et al. 1988). However, interpretation in terms of abundance is still uncertain because of similar excitation considerations to those affecting the 183 GHz line. A similar situation applies to the recently detected 321 GHz (10_{29}–9_{36}) transition (Menten, Melnick, & Phillips 1990) which provides information about the radiative environment of water, but not about its abundance.

Using infrared techniques, Knacke, Larson, & Noll (1988) have used the KAO to measure a vibration-rotation absorption line of water ($\nu_3\ 1_{01}$–2_{02} at 3801 cm^{-1}) toward Orion A, but the result even from KAO altitudes is limited by telluric water. The reported water abundance toward the BN object is $H_2O/CO \leq 0.01$–0.08 based on a 2–4 σ measurement on the side of the telluric line.

Additional estimates for the water abundance are based on observations of HDO (Phillips, Jefferts, & Wannier 1973; Olofsson 1984; Moore, Langer, & Huguenin 1986; Plambeck & Wright 1987; Jacq et al. 1990) and, possibly, of H_3O^+ (Hollis et al. 1986; Wootten et al. 1986). However, interpretation of these results is also uncertain. The HDO lines yield a water abundance only via a quantitative model of the chemical fractionation of deuterated species. The H_3O^+ results yield a water abundance only via quantitative chemistry models: in particular, the branching ratio of the H_3O^+ recombination reaction and the rate of destruction of water by ion-molecule reactions.

Observations of a ground-state transition are clearly needed. Even in the absence of population inversion, high-level transitions such as those discussed above are difficult to interpret

[1] Jet Propulsion Laboratory, California Institute of Technology, 4800 Oak Grove Drive, Pasadena, CA 91109.
[2] Observatoire de Paris, Meudon, France.
[3] Also Ecole Normale Superieure de Paris, France.

because the observed line strengths are very sensitive to the assumed physical properties of the sources. In LTE, a relatively modest change in the cloud kinetic temperature from 40 to 150 K produces a factor of 80 change in the intensity of the 380 GHz (4_{14}–3_{21}) transition, but only a factor of 1.6 change in the 548 GHz (1_{10}–1_{01}) transition reported below. For non–LTE conditions, the sensitivity of the high-level transitions is likely to be even larger. Molecular cloud cores are known to be nonuniform, displaying large internal variations in density, infrared luminosity, and kinetic temperature. Temperatures may vary from 15 K in quiescent clumps to 1000 K in shocked gas. Therefore, the higher levels are troublesome to interpret because small column densities of excited material can produce the same apparent line intensity as very large column densities unexcited material. The problems for the higher lying energy states are further complicated by non–LTE excitation, giving rise to negative excitation and maser emission at 22 GHz (6_{16}–5_{23}), 321 GHz (10_{29}–9_{36}), 183 GHz (3_{13}–2_{20}), and 380 GHz (4_{14}–3_{21}).

The 1_{10}–1_{01} transition is especially useful for astrophysical research because it is the ground-state transition of ortho-water. The line of $H_2{}^{16}O$ is not observable from the ground, or even from airplane altitudes because of blockage by atmospheric water. Fortunately, it is possible to observe the rare ^{18}O form of water from the operating altitude of the G.P. Kuiper Airborne Observatory (KAO): 39,000–45,000 (11.9 ~ 13.7 km). Comparison to the optically thin $C^{18}O$ rotational lines then directly yields the desired H_2O/CO ratio.

2. OBSERVATIONS

In this paper we report on interstellar observations of the 548 GHz (1_{10}–1_{01}) line of $H_2{}^{18}O$. The source list, given in Table 1, includes the central regions of seven giant molecular clouds and two late-type stars. The observations were made at the Nasmyth focus of the 91 cm Cassegrain KAO telescope during five flights from Moffett Field, California: three in 1987 February and two in 1987 December.

2.1. *Instrumentation*

The receiver system consisted of two orthogonally polarized channels operating at, respectively, 548 and 183 GHz in 1987 February and at 548 and 372 GHz in 1987 December. The two wavelengths were separated by a polarizing grid. Results from the 183 and the 372 GHz systems have no direct bearing on the present paper, except in providing additional pointing and calibration checks. The observation of a strong, broad-winged 183 GHz water profile in Orion A simultaneous to the 548 GHz observations provides confidence about the correctness of the telescope pointing. The pointing of both receivers was checked independently with the Moon as a source.

The 548 GHz receiver was a self-contained unit about 20 cm on a side, containing an uncooled double-sideband, subharmonically pumped GaAs diode mixer, a multiplied ($\times 3$) phase-locked Gunn diode local oscillator, and a polarizing Michelson interferometer serving as a single-sideband filter (Taylor et al. 1985). The 548 GHz unit was mounted on a receiver plate, containing lower frequency receivers, secondary optics, polarization splitter, phase wobbler, and ambient/cold calibration loads (Fig. 1). The 548 GHz system temperature, referred to the entrance of the telescope cavity, was $17{,}500 \pm 500$ K (SSB) for the 1987 February flights and $14{,}800 \pm 500$ K for the December flights, the difference arising from differences in vignetting and the extent of cold spillover, and from ambient water vapor. Because the main telescope is at the low atmospheric pressure exterior to the aircraft, the only significant absorption is within the receiver system, which operates at cabin pressure. This attenuation degrades the system noise temperature, but not the calibration, since the calibration loads were located close to the pressure window into the telescope. At the operating cabin altitude of 8000 feet (2.4 km) and low relative humidity during the actual flights, it is thought that the attenuation within the receiver was not more than 10%, and thus increased the system noise by less than 1800 K.

The spectral line backend used for the 548 GHz observations was a 256 channel filter bank with 1 MHz filters. We also used a developmental acousto-optical spectrometer (AOS) having a 430 MHz total bandwidth with ~2–3 MHz resolution.

The 183 GHz channel, useful as a pointing/calibration check, was essentially the same as on prior KAO flights (KK), consisting of a double-sideband GaAs Schottky mixer cooled to approximately 15 K by a closed cycle helium refrigerator. When cooled, it had a single-sideband noise temperature of 750 K. The mixer was operated uncooled for the February 19 flight because of airplane power problems. Uncooled, the 183 GHz channel had a 2600 K single-sideband noise temperature. The 372 GHz receiver was housed in the same Dewar as the 183 GHz receiver and provided receiver SSB noise temperatures of 1300 K during the first December flight and 1800

TABLE 1

SOURCE LIST

Source	R.A.(1950)	Decl.(1950)	V_{lsr} (km s^{-1})	T_{rot} (K)	Δv (km s^{-1})	n (cm^{-3})	Size	Comments
DR 21	$20^h37^m13^s$	42°08′51″	−1	...	...	...	...	
NGC 7538	23 11 37	61 11 54	−56	...	...	...	...	IRS 1, 2, 3
W3	2 21 43	61 52 49	−35	...	...	...	...	IRS 4
Orion A:	5 32 47	−5 24 15	...	...	...	...	...	IRS 2
Extended Ridge	...	...	9	80	4	10^5	>150″	
Compact Ridge	...	...	7	100	4	$>10^6$	25	
Plateau	...	...	7	180	40	$>3 \times 10^6$	20	
Hot Core	...	...	3–5	300	8	$>10^7$	8	
NGC 2024	5 39 15	−1 56 30	10	45	2	$>10^6$	> 150	
Mon R2	6 05 20	−6 22 30	10.5	...	...	...	...	
NGC 2264	6 38 25	9 32 29	5, 8	27	3	3×10^5	>150	AFGL 989
R UMa	10 41 08	69 02 19	38	...	...	...	...	
Y UMa	12 38 05	56 07 12	0	...	...	...	...	

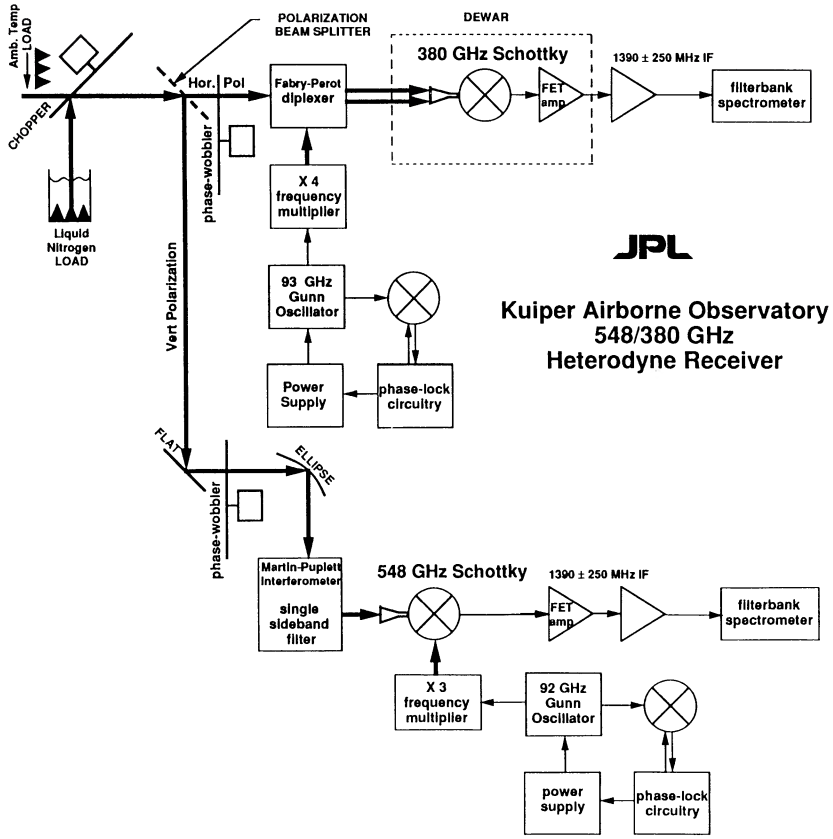

FIG. 1.—Block diagram of the JPL 548/380 GHz receiver. For the flights using a 183 GHz receiver, the same diagram applies with the change of 380 for 183.

K during the second flight. The reduced sensitivity in the second flight resulted from a leak in the Dewar, resulting in water condensation on the Dewar window.

2.2. *Observing Technique*

Most of the observations from the February flight were made using a double-switching technique to achieve adequate spectral baselines. A 4 Hz rotating chopper was used to switch emission from the sky against that from a microwave absorber cooled by liquid nitrogen (load-switching). This single-switching technique allows the telluric water lines to be monitored in individual scans (cf. Fig. 2), serving to confirm operation of the receiver and to provide some real-time information about the atmospheric opacity (see below). For the astronomical observations, load-switched scans were obtained both on- and off-source and the difference spectra reported here. In December, another double-switching technique was used: a chopping secondary was used (beam-switching) with a throw of 11′23″, alternating the reference and source with respect to the beams. Spectra could then be subtracted by pairs to remove any residual baseline effects. This scheme had the advantage of doubling the integration time on-source.

The success of both double-switching strategies can be appreciated by noting that spectral baselines were not removed from any of the reported data. For one source only (R Mon) spectral channels have been removed to eliminate interference spikes in the data.

2.3. *Atmospheric Effects*

At the KAO operating altitudes of 11.9–13.7 km (39,000–45,000 ft), there are two dominant and approximately equal sources of atmospheric opacity, the 1_{10}–1_{01} transitions of $H_2{}^{18}O$ and $H_2{}^{16}O$. In both cases, the opacity varies across the observing passband because of the atmospheric spectral line shape, resulting from atmospheric broadening (3.3 GHz atm^{-1}) throughout the overhead atmosphere. The $H_2{}^{18}O$ opacity accounts for approximately 60% of the measured opacity and is peaked at the rest frequency of the line (Fig. 3).

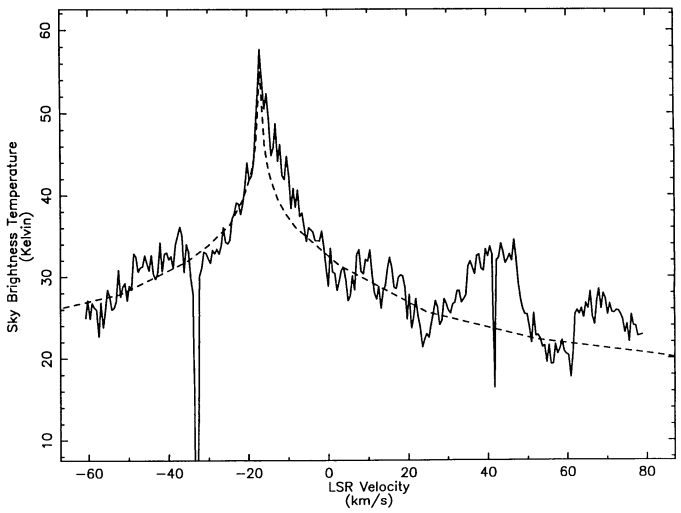

FIG. 2.—Observations are presented in an unswitched form to show the telluric water feature: summing rather than differencing the on- and off-source spectra. The $H_2{}^{18}O$ line is shown at its expected intensity based on a standard model atmosphere.

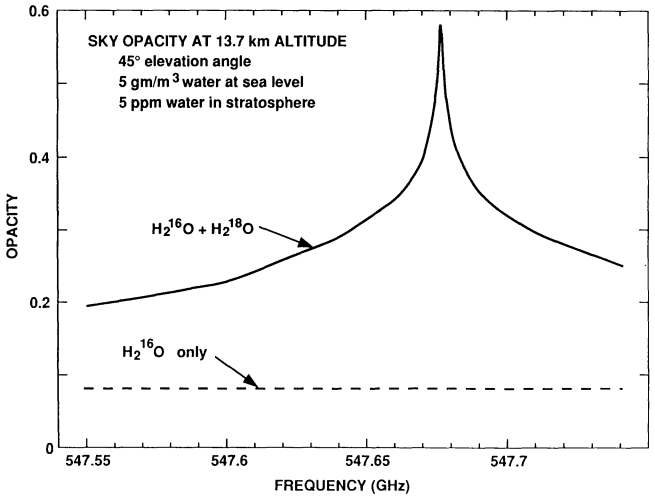

FIG. 3.—The calculated atmospheric opacity is shown near 548 GHz. Because the $(1_{10}–1_{01})$ line of $H_2{}^{18}O$ lies in the far pressure-broadened wing of the dominant absorber, $H_2{}^{16}O$, significant reductions in opacity at 548 GHz arise from a decrease in pressure. This fact explains the significant absorption within the receiver optics operating at cabin pressure, without a large analogous atmospheric blockage (see text).

The opacity half-width spans 0.8 GHz even at KAO altitudes. The $H_2{}^{16}O$ opacity arises from the analogous transition at 557 GHz, and is only slightly sloped across our 400 MHz bandpass, decreasing toward longer wavelengths. The opacity model has two inputs: the tropospheric water content and the stratospheric one. The calculation represented in Figure 3 assumed a sea level humidity of 5 g m^{-3}, distributed up to an altitude of 15 km with a scale height of 2 km. Above that, the assumed stratospheric mixing ratio was taken to be 5 ppm. The resulting opacity is calculated for a 45° elevation angle. The resulting opacity model, not adjusted to fit the KAO data, is compared to the observed sky brightness in Figure 2. The KAO observations are based on spatially unswitched data, so that details in the spectrum could be easily ascribed to baseline defects. The input model parameters were based entirely on standard atmospheric models and prior estimates of the atmospheric water distribution, not adjusted at all to the observations. Thus the very good agreement between the observations and the model is a bit fortuitous.

2.4. *Telescope Calibration*

The telescope gain and efficiency (Table 2) were checked before flight by measuring the system response to liquid nitrogen absorbers placed at different positions in the optical train, and the results were checked by means of lunar observations during one of the actual flights. The forward efficiency of the telescope was limited by the thick mylar pressure window separating the pressurized cabin from the telescope cavity. A check of the telescope illumination was performed between the second and third flights in the February run. A slight realignment was made at that time, which improved the performance during the subsequent flights from an aperture efficiency of 31% to one of 37%. This did not significantly effect the antenna beamwidth, which was $\approx 2'.7$ throughout, nor did this correction affect the forward efficiency (η_f), defined to be the response of the system to any radiation entering the forward 2π st of the telescope (main beam, sidelobes, and forward scatter) relative to the total response. The illumination pattern from the receiver system was measured to be a circular Gaussian with a 16 dB illumination taper at the edge of the secondary reflector. As a result of the illumination correction, the data from the first two flights were scaled by a factor of 1.2 and all intensities reported as though taken with the correctly aligned system. The small misalignment did not affect the effective telescope pointing.

The telescope focus and pointing for the submillimeter instrument were set, relative to a fixed reference camera, before the actual flights. Active (in-flight) pointing and focus were made using a reference camera on available bright stars. In December, the pointing was checked using the Moon and Jupiter. Due to an initial error in the interpretation of the December 9 pointing data (involving the sense of linear polarization), the pointing error was actually increased somewhat in the second half of the December 9 flight. This error was corrected in the December 11 flight. Estimated pointing errors are given in Table 2.

3. ANALYTICAL APPROACH

3.1. *Spectroscopy of Water*

Both ^{16}O and ^{18}O water exist in ortho and para states, with statistical weights of 3 and 1 respectively, due to the alignment or antialignment of the spins of the two hydrogen nuclei. The two spin states are not radiatively coupled, giving rise to two

TABLE 2

TELESCOPE PARAMETERS

PARAMETER	DATE (1987 UT)				
	Feb 19, 20	Feb 25	Dec 9	Dec 9	Dec 11
Objects	Orion A NGC 2264 NGC 2024 Y UMa W3 Mon R2	W3 Orion A NGC 2264 R UMa	NGC 7538 W3 Moon Jupiter	Orion A NGC 2264	DR 21 NGC 7538 W3 Orion A NGC 2264
Beamwidth	2'.7	2'.7	2'.7	2'.7	2'.7
Pointing error	<1'.5	<1'.5	0'.6	1'.4	<0'.3
Forward efficiency (η_f)	0.53	0.53	0.53	0.53	0.53
Forward scatter and spillover efficiency	0.66	0.79	0.79	0.79	0.79
Main beam efficiency	≤0.90	0.90	0.90	0.90	0.90
Aperture efficiency	≤0.31	0.37	0.37	0.37	0.37
Gain correction	2.35	2.35	1.15	2.35	1.00

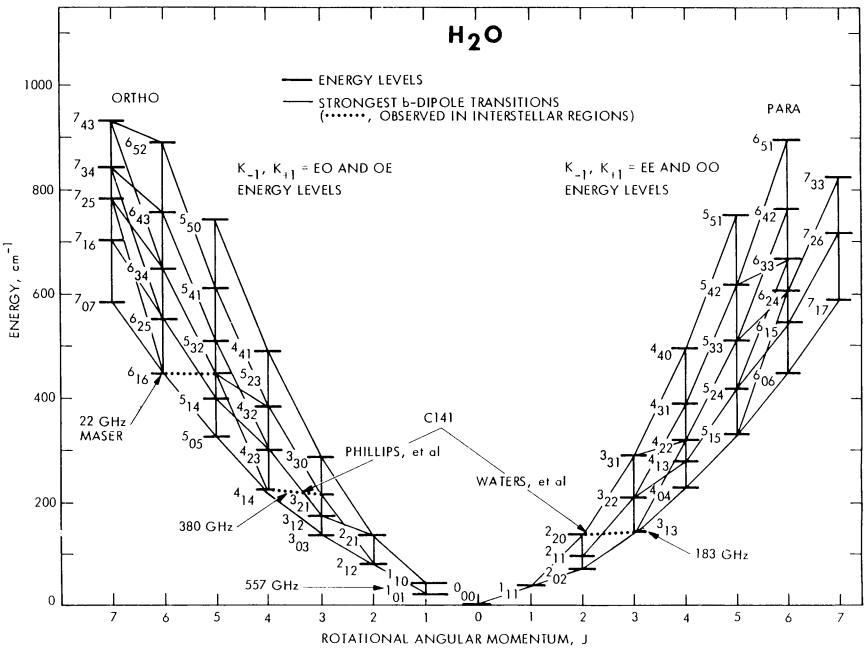

FIG. 4.—Energy level diagram of H_2O. Although the diagram shows the energy levels of the common ^{16}O form, the diagram for ^{18}O water is quite similar because (1) the nuclear spins of the two oxygen nuclei are the same and (2) the energy levels are dominated by the light H nuclei rather than the heavier O. The observed water transitions at 22, 183, and 380 GHz are shown, as well as the unobserved water transition at 557 GHz which is the analog to the 548 GHz transition discussed here.

independently excited sets of energy levels (Fig. 4). Thus, from the point of view of molecular excitation, there are two effective ground states: the 1_{01} state of ortho-water and the 0_{00} state of para-water. The 1_{01} state of $H_2{}^{18}O$ is also the lower energy level of the 548 GHz transition. The rotational constants are listed in Table 3 along with the line strengths (De Lucia, Helminger, & Kirchhoff 1974). These line strengths are defined as:

$$S = (2J + 1)|\mu_{J' \leftarrow J''}|^2/\mu^2 , \quad (1)$$

where $|\mu_{J' \leftarrow J''}|$ is the dipole moment matrix element connecting the upper (′) and lower (″) states. The statistical weight of each rotational state must be considered when calculating the spectral intensities: 3 for the 548 GHz line of $H_2{}^{18}O$ and 1, for example, for the 183 GHz line of $H_2{}^{16}O$.

Figure 4 shows the energy level diagram for $H_2{}^{16}O$. The diagram for $H_2{}^{18}O$ is similar but with slightly different energies due to the larger mass of the ^{18}O nucleus (Table 3). The three radiofrequency lines of water (22, 183, and 380 GHz) which have been observed to date are marked on Figure 4. As can be seen, these lines arise from energy levels high compared to cloud kinetic temperatures which correspond to about 21 cm^{-1} (30 K).

TABLE 3

ROTATIONAL SPECTRUM OF WATER

A. ROTATIONAL CONSTANTS

Rotational Constants (MHz)	$H_2{}^{16}O$	$H_2{}^{18}O$
B_x	835,840	825,366
B_y	435,351	435,331
B_z	278,138	276,950

B. OBSERVED TRANSITIONS AND ENERGY LEVELS

	$H_2{}^{16}O$			$H_2{}^{18}O$		
STATE	Frequency (MHz)	E_{lower} (cm^{-1})	S	Frequency (MHz)	E_{lower} (cm^{-1})	S
1_{10}–1_{01} ortho	556,936.00	23.794	1.500	547,676.44	23.754	1.500
4_{14}–3_{21} ortho	380,197.37	212.157	0.123	390,607.76	210.795	0.119
3_{13}–2_{20} para	183,310.09	136.164	0.102	203,407.52	134.780	0.100
6_{16}–5_{23} ortho	22,235.08	446.511	0.057	5,625.15	445.155	0.053

NOTES.—Data from De Lucia, Helminger, & Kirchhoff 1974. The states with the second two (subscripted) quantum numbers even-even or odd-odd are para, with statistical weight 1. The even-odd and odd-even states are ortho with weight 3.

3.2. *Molecular Excitation and Spectral Line Formation*

In the subsequent four sections, we develop the analytic tools to interpret the (lack of) water emission of 547 GHz. We consider the collisional excitation and treat the transfer of millimeter-wave radiation in detail. Because of grave uncertainties in the ambient infrared flux, we do not consider infrared excitation of the line, but note that our derived upper limits to the water abundance are all the more conservative by not modeling the infrared excitation. We find that collisionally excited water emits 547 GHz radiation primarily from regions where the excitation temperature is very much less than the gas kinetic temperature. This allows for certain simplifying assumptions to be made when interpreting the emergent line radiation. In the following sections, we develop a model for the emergent line intensity. In a simple slab model, the emergent line intensity can be analytically related to the number of exciting collisions. For dense cloud cores an LVG model is applied to a centrally dense spherical cloud. The LVG model used was also applied to a single-component model and found to agree with the analytic result to within 20%.

3.2.1. *Radiative and Collisional Constants*

The water molecule has a permanent dipole moment of 1.8546 ± 0.0004 D (Clough et al. 1973; Dyke & Muenter 1973) applying to both the ^{18}O and ^{16}O forms. The two rates of interest for computing rotational excitation are those for spontaneous emission and for collisional excitation and deexcitation (the same to within a Boltzmann factor). The spontaneous emission rate is calculated from the measured transition strength S in Table 3, yielding $A_{ul} = 0.033\ s^{-1}$. Collisional excitation rates are computed theoretically from known molecular parameters. We use the computations of the H_2O-He cross-sections by Palma et al. (1988, 1989), improving on earlier values of Green (1980), which used less accurate interaction potentials. The important, low-temperature collision rate constants are listed in Table 4. It is assumed that the rate constant of the dominant H_2O-H_2 collisions is a factor 1.4 larger than the tabulated H_2O-He collision rate constants, corresponding to the larger thermal velocity of H_2 compared to He (Green & Thaddeus 1976).

Compared to longer wavelength molecular lines, the half-millimeter water line has a large spontaneous emission rate which, combined with the moderate energy of the transition, is what makes water an effective coolant of the interstellar medium. It also leads to large opacities since B_{lu} is proportional to A_{ul}, and except at very high densities, leads to a very significant role for molecular excitation by photon trapping.

3.2.2. *Line Emission in the Case of Low Excitation*

At a gas kinetic temperature of 100 K, the 1_{10} level population approaches collisional thermalization when the downward collision rate, C_{ul}, is higher than the spontaneous radiative rate, A_{ul}. This corresponds to a density, $n(H_2)$, of $7 \times 10^9\ cm^{-3}$, larger than observed except, perhaps, for small embedded protostars. At smaller densities, and the high expected opacities, photon trapping within a cloud increases the excitation temperature, and the emergent line intensity, T_{RJ}, increases linearly with opacity so long as $C_{ul} \times \tau \ll A_{ul}$ (cf. Penzias 1975). Molecular excitation by radiation from embedded dust (assuming a normal gas/dust ratio of 90), is not significant if $T_{kin} > 30$ K, the normal situation for the observed sources (and close enough for NGC 2264 with $T_{kin} = 28$ K).

Therefore, even where photon trapping is important ($\tau \gg 1$), the emergent emission line brightness can still be related to a water abundance so long as $C_{ul} \times \tau \ll A_{ul}$, in which case the emission-line brightness temperature, T_{RJ}, is small compared to the gas kinetic temperature, T_{kin}. In that case, it can be assumed that every upward (1_{01} to 1_{10}) collisional transition produces a line photon which eventually escapes from the cloud.

In this case, the observed line intensity can be simply related to the water abundance for a volume of known, constant density and temperature. For the high densities relevant to water emission, the sources are generally smaller than the KAO beam of 2'.7. So, assuming

$$C_{ul} \times \tau \ll A_{ul} \tag{2}$$

and

$$r_{source}/R_{source} \ll \lambda/r_{KAO}\ , \tag{3}$$

we get

$$T_A = A_e hcc_{H_2O\text{-}He} r_{source}^3 n^2(H_2) X_{mol}/6kR_{source}^2 \Delta v \tag{4}$$

where

$$X_{mol} = [\text{ortho-}H_2{}^{18}O]/[H_2]$$
$$= [H_2O]/[H_2] \times [^{18}O]/[^{16}O] \times [o]/[o + p]\ , \tag{5}$$

$$c_{H_2O\text{-}He} = \langle v\sigma(v) \rangle\ , \tag{6}$$

and

$$A_e = \eta_A \pi r_{KAO}^2 \tag{7}$$

is the effective area of the KAO aperture. In the above expressions, r_{source} and R_{source} are the radii and distance to the molecular source, r_{KAO} is the radius of the KAO telescope, $c_{H_2O\text{-}He}$ is the collision rate constant (as in Table 4), v is the relative thermal velocity of H_2 and water, $\sigma(v)$ is the collision cross section, η_A is the KAO aperture, $n(H_2)$ is the hydrogen volume density, Δv is the spread in source velocity, and c, h, and k have their usual meanings. Equation (4) is strictly true only for a rectangular line profile (constant intensity), but corrections for line shape are small for the simple profiles which apply to the observed sources.

As an example, we pick an Orion-like source which just fills the KAO beam, with $R_{source} = 500$ pc, $\Delta v = 3\ km\ s^{-1}$, $n(H_2) = 10^5\ cm^{-3}$, and $T_{kin} = 100$ K. The result is $T_A = 0.3$ K for $X_{mol} = 4.5 \times 10^{-8}$ and $\eta_A = 0.37$. For regions where the opacity becomes too large, we evaluate the emission-line intensity by means of the Sobolev approximation. In the following sections, we discuss (1) the Sobolev approximation and (2) an analysis of a centrally dense star-forming region. We have evaluated $H_2{}^{18}O$ column densities assuming collisional excitation and discuss briefly the possible effects of infrared excitation.

TABLE 4

LOW-TEMPERATURE COLLISION RATE CONSTANTS

T_K (K)	$C_{H_2O\text{-}He}$ ($cm^3\ s^{-1}$)
20	5.2×10^{-13}
30	1.1×10^{-12}
50	2.6×10^{-12}
100	7.0×10^{-12}

In any condition of molecular excitation, the optical depth, τ, can be written in terms of the population of the lower energy level as

$$\tau = (g_u/g_l)[c^2 A_{ul} N_l \phi(\Delta v)/8\pi v^2](1 - e^{T_*/T_{ex}}) \quad (8)$$

where the g's are the state multiplicities, u and l refer to the upper and lower energy levels, T_* is hv/k, ϕ is the normalized line shape function, and the other symbols have their usual meanings. The relation of N_1 to N_T, the total molecular column density relies on knowledge of the excitation of the entire rotational ladder.

3.2.3. *The Sobolev Approximation: Photon Trapping*

We have used an LVG code to compute the equivalent Rayleigh-Jeans brightness temperature of the 548 GHz line (Scoville & Solomon 1974; Goldreich & Kwan 1974), and the results are shown in Figure 5, where the vertical axis is the emergent line intensity, given in terms of its equivalent Rayleigh-Jeans brightness temperature T_{RJ}. The code is a simple one, assuming a plane-parallel geometry and assuming $v \propto r$. The horizontal axis is proportional to the effective column density of water in each velocity resolution element but is related to quantities of direct significance: the assumed H_2O/CO ratio and the velocity behavior. Thus:

$$(H_2O/CO)/(dv/dr) = N(H_2O) \times v/[n(H_2) \times \Delta v \times c \times f(CO)] \quad (9)$$

where f(CO) is the (observable) CO abundance, Δv is the spectrometer frequency resolution, v is the spectral line frequency, and c, $n(H_2)$, and $N(H_2O)$ have their usual meanings. At the densities of interstellar clouds, the 1_{10} upper level is very sparsely populated, so that varying the water abundance [fixing $n(H_2)$] has an identical effect on the line brightness as varying the density, $n(H_2)$ (holding the total water abundance fixed). Both variations effectively modify the number of exciting collisions. The emission also changes with temperature, especially in cool gas ($T < 100$ K).

3.2.4. *Line Formation in a Centrally Dense Core*

The dense cores of the molecular clouds are not uniformly dense. Presumably, they have a hierarchical density structure, with most of the volume filled by lower density gas and less of the volume filled with the high-density gas. For a given molecular transition, the emergent line intensity can be summed over all density regimes under either of two conditions: (1) the cloud satisfies the LVG criterion, or (2) the overlying opacity does not exceed the ratio of the Einstein A-coefficient to the de-exciting collision rate, C_{ul}. With this in mind, we estimate the density regime giving rise to the dominant 1_{10}–1_{01} emission by using an empirical density model and the LVG analysis given above. However, we note that such an approach is robust in the sense that, within the KAO beamwidth, it does not matter whether or not the LVG assumption is strictly satisfied, so long as the line photons escape. Because of the very low collision rate (compared to the radiative rate), such escape is greatly facilitated.

Many molecular cloud cores, including those observed in this paper, can be fitted by a relatively simple model first derived for the Orion A molecular cloud by Goldsmith et al. (1980). From a variety of data (CO, CS, H_2CO, and NH_3), they have estimated a density of gas at 1.2 from IRc2 to be $\sim 10^5$ cm^{-3} and have fitted a density law to the denser gas corresponding to an r^{-2} density relation ($n = 1.4 \times 10^5$ cm^{-3} r^{-2}, where r is in arcmin). In the case of the KAO (2.7 diameter HPBW), that implies that a density of $\sim 10^5$ cm^{-3} applies to our whole beam, 2×10^5 cm^{-3} applies to half our beam, 4×10^5 cm^{-3} to one-quarter of our beam, etc. Regardless of the detailed geometry, it is the assumed distribution of gas into different density regimes which is important in modeling the integrated emergent line intensity.

Table 5 presents the source brightness, $T_{R\text{-}J}$, and observed KAO brightness temperature, T_A, for such a stratified model, taking account of the small beam-filling factors for the highest densities. The results in Table 5 assume $dv/dr = 3$ km s^{-1} pc^{-1}, $T_K = 80$ K, and $^{16}O/^{18}O = 500$. Three different fractional

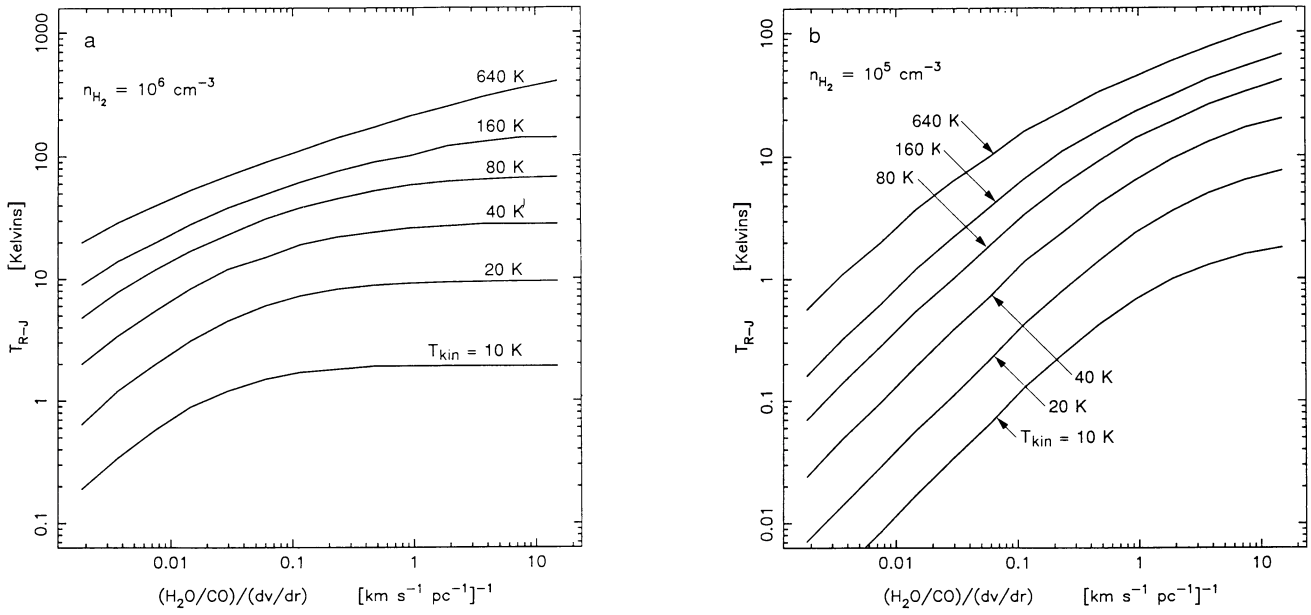

FIG. 5.—Results of an LTE analysis are presented for gas densities, $n(H_2)$ of 10^5 and 10^6 cm^{-3}, and kinetic temperatures of 10, 20, 40, 80, 160, and 640 K. The vertical axis is the emergent line intensity, given in terms of its equivalent Rayleigh-Jeans brightness temperature T_{RJ}. The horizontal axis is proportional to the effective column density of water in each velocity resolution element, related to quantities of direct significance.

TABLE 5

EMISSION FROM A CENTRALLY DENSE CORE

	H_2O/CO								
	0.030			0.010			0.003		
n_{H_2} (cm^{-3})	T_{R-J} (K)	τ	T_A (K)	T_{R-J} (K)	τ	T_A (K)	T_{R-J} (K)	τ	T_A (K)
1×10^5	0.37	64	0.37	0.13	22	0.13	0.04	6.5	0.04
2×10^5	1.37	119	0.68	0.49	42	0.25	0.15	13	0.08
5.0×10^5	6.02	224	1.20	2.59	91	0.52	0.89	31	0.18
1.0×10^6	14.1	302	1.41	7.3	139	0.73	3.00	53	0.30
2.0×10^6	26.5	370	1.33	16.4	182	0.82	8.2	80	0.41
5.0×10^6	46.2	495	0.92	34.3	236	0.69	21.9	110	0.44
1.0×10^7	58.1	717	0.58	49.0	304	0.49	36.3	133	0.36
2.0×10^7	64.4	1228	[0.32][a]	60.0	457	0.30	50.8	174	0.25
5.0×10^7	66.7	2895	[0.13][a]	65.8	988	[0.14][a]	62.9	318	0.13
Total KAO intensity			6.5			3.9			2.2

[a] For the bracketed values, $C\tau/A > 0.5$ in the overlying material. In that case, collisional de-excitation in the overlying gas is likely to prevent the escape of photons and the conservative approach is taken to simply not add T_A into the total observable KAO intensity.

water abundances are used: $H_2O/CO = 0.030$, 0.010, and 0.003. In all three cases, the dominant emission comes from densities ranging from 1 to 5×10^6 cm^{-3}, with line opacities in the range 100–200. Despite the large overlying water opacities, collisional de-excitation will be rare and line photons will eventually escape. Of course, depending on the velocity behavior, there can be appreciable spatial diffusion of the source, much as the light emitted from the hot filament of a light bulb is diffused by its diffusive glass envelope. For a true large-scale velocity gradient, this effect is very small. In the case of the 2'.7 beamwidth of the KAO, the density filling the beam is never larger than 4×10^5 cm^{-3}, and it is therefore unlikely that the observed intensity is much affected by such diffusion.

In deriving abundances from such a model, three input parameters (aside from the water abundance) are needed: the kinetic temperature, the velocity gradient, and the assumed space density at some fixed diameter, conveniently taken to be the diameter of the KAO beam. Equation (4) predicts (and our model calculations have reconfirmed) that for typical source parameters, the inferred water abundance for a fixed intensity upper limit, varies as (1) $1/T_{kin}$; (2) linearly with the assumed velocity gradient, dv/dr and (3) as $1/n_0^2$, where n_0 is the space density at the edge of the KAO beam. The variation of source brightness with assumed abundance is shown in Table 5.

3.2.5. *The Ortho/Para Ratio and Isotope Fractionation*

The present observations measure the abundance of ortho-water. How accurately does this reflect the total water abundance? To get a total abundance, we must multiply by $(1 + p/o)$, where p/o is an assumed para/ortho ratio. One possible assumption is to assume that the two states are populated according to their relative statistical weights of 1/3, yielding $(1 + p/o) = 4/3$. A more conservative approach is adopted, assuming thermodynamic equilibrium between the two states at the gas kinetic temperature, yielding $(1 + p/o)$ larger than 4/3. In practice, this assumption does not significantly affect our results because the 1_{01} ortho ground state is so close (23.7 cm^{-1}) to the 0_{00} para ground state. The factor $(1 + p/o)$ never varies by more than 5% for temperatures greater than 30 K.

The present observations measure the abundance of the relatively rare $H_2{}^{18}O$ form. How does that relate to $H_2{}^{16}O$? The answer has two parts. First, the most meaningful comparison is to the ubiquitous CO molecule, and that is also best measured using the rare ^{18}O variant because of the large interstellar opacity of $C^{16}O$. In that case, knowledge of the $^{18}O/^{16}O$ ratio is not needed. Where we infer the total water fraction (H_2O/H_2), we use $^{16}O/^{18}O = 500$: its terrestrial value and the one which apparently also applies to interstellar clouds (cf. Wannier 1980). The only possible problem could arise in the event of selective isotope fractionation. Fortunately, oxygen is not thought to be significantly fractionated either in water or in CO: the former because the free energy associated with isotope exchange is smaller than $k \times T_K$ and in the latter because of the lack of plausible exchange reactions.

4. RESULTS

The source list contains seven giant molecular clouds (GMCs) and the circumstellar shells surrounding two OH/IR stars noted for their strong 22 GHz water maser emission (Table 1). Results are presented in Figure 6 and Table 6. The primary purpose of the present observations was to determine the water abundance in GMCs. The two stars were observed during the February flights, when flight constraints produced a flight leg without available GMCs. A complete analysis of the circumstellar results is deferred until a later paper.

4.1. *Orion A*

The Orion source is known to have a complex structure. Within the KAO beamwidth there are several kinematic components which are widely recognized, though the distinction between them in fact is not always clear (see, e.g., Blake et al. 1987). These components include (1) the Extended Ridge, (2) the Compact Ridge, (3) the Plateau Source, and (4) the Hot Core. Approximate physical parameters for these four sources are given in Table 1. Our measured upper limit applies to all components simultaneously, limiting the water abundance, respectively, in cool, shocked, and warm cloud environments. Because the Plateau material is kinematically (and, therefore chemically) distinct from the other components, we treat it independently. Otherwise, we evaluate the results for Orion as a single component of width 4–6 km s^{-1}. In practice, the non-

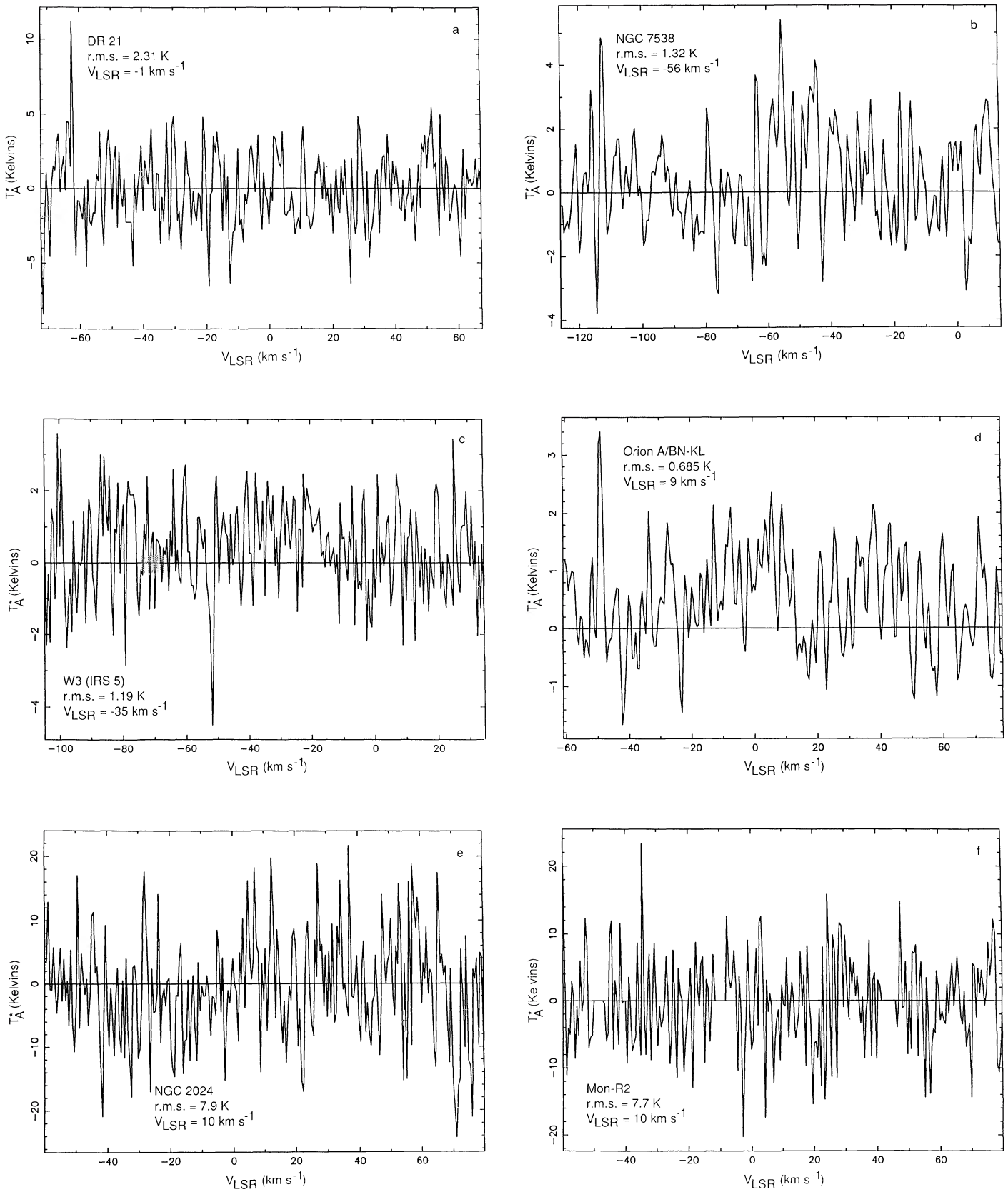

FIG. 6.—Spectra of $H_2{}^{18}O$ at 548 GHz are shown for the observed objects. The spectra are fully corrected for atmospheric and telescope losses. There has been no spectral baseline removal other than to adjust the zero levels in two sources. In one object (R Mon) some channels have been removed because of IF interference. In the other sources all channels are plotted.

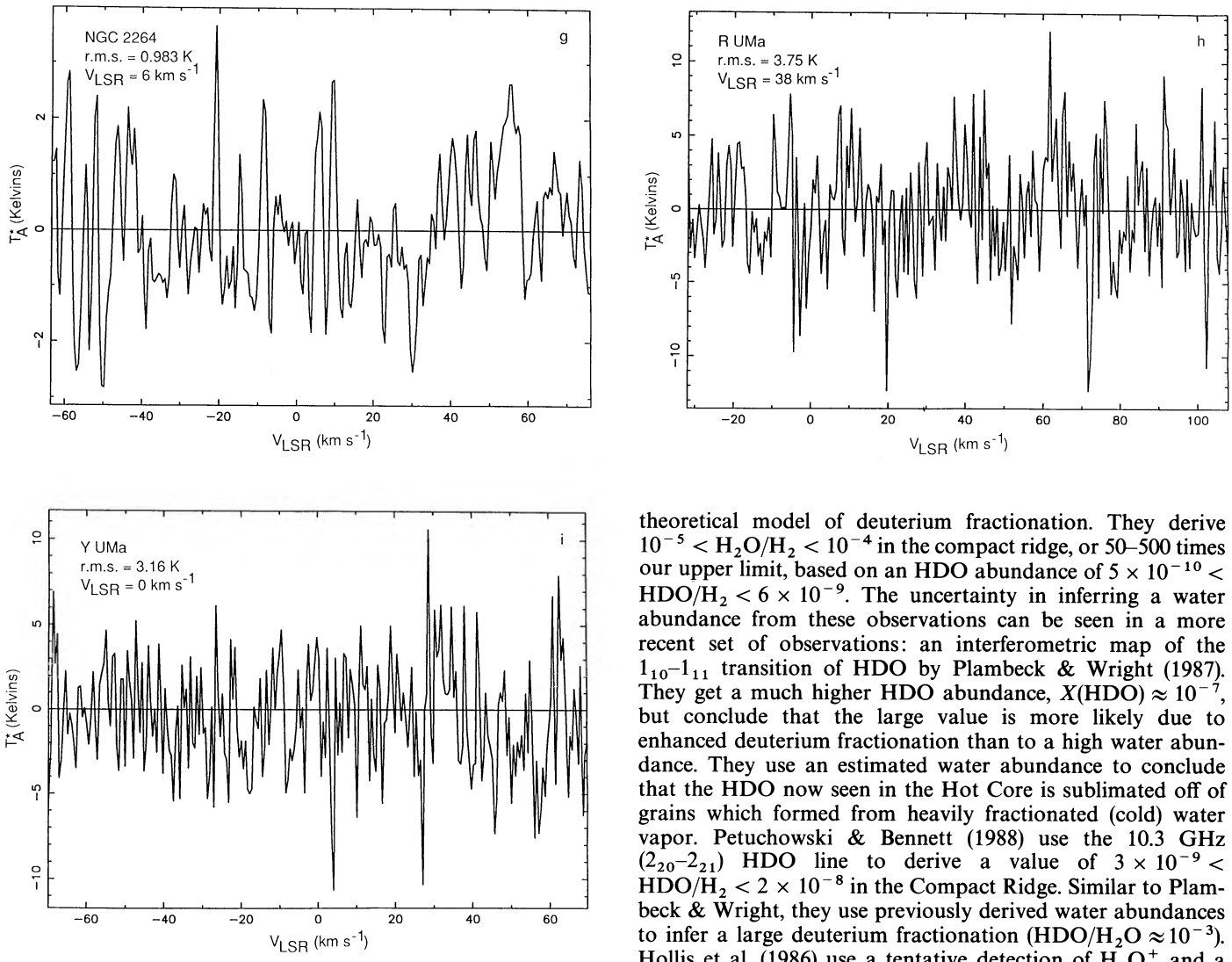

FIG. 6—*Continued*

plateau limit is most directly applicable to the denser, warmer material in the Hot Core and the Compact Ridge, which contribute most significantly to the emission-line strength.

4.1.1. *The Extended Ridge, Compact Ridge, and Hot Core*

In the nonplateau material, Table 5 offers a way to evaluate our upper limit. The rms noise level on our 1_{10}–1_{01} $H_2{}^{18}O$ line in Orion A is 0.9 K in the 1 MHz channels, and the integrated line intensity over a 6 km s^{-1} line width centered on $v_{LSR} = 9$ km s^{-1}, is 3.6 ± 1.6 K km s^{-1}, yielding a 3 σ upper limit of 2.5 K or a possible 2 σ detection, depending on how it is viewed (Table 6). From Table 5, we can set an upper limit to the water abundance of $H_2O/CO < 0.003$, or $H_2O/H_2 < 2 \times 10^{-7}$, a 3 σ result. The marginal detection, if genuine, would imply an actual H_2O/CO ratio of ≈ 0.001.

These values can be directly compared to other estimates. Waters et al. (1980) used the 3_{13}–2_{20} transition at 183 GHz to infer a larger water abundance: $H_2O/CO = 0.005$–0.05. However, these earlier results are thrown in doubt due to subsequent results showing the line to be a maser. Moore et al. (1986) derive H_2O/H_2 for the Compact Ridge based on observations of the 1_{10}–1_{11} and 2_{11}–2_{12} lines of HDO and on a theoretical model of deuterium fractionation. They derive $10^{-5} < H_2O/H_2 < 10^{-4}$ in the compact ridge, or 50–500 times our upper limit, based on an HDO abundance of $5 \times 10^{-10} < HDO/H_2 < 6 \times 10^{-9}$. The uncertainty in inferring a water abundance from these observations can be seen in a more recent set of observations: an interferometric map of the 1_{10}–1_{11} transition of HDO by Plambeck & Wright (1987). They get a much higher HDO abundance, $X(HDO) \approx 10^{-7}$, but conclude that the large value is more likely due to enhanced deuterium fractionation than to a high water abundance. They use an estimated water abundance to conclude that the HDO now seen in the Hot Core is sublimated off of grains which formed from heavily fractionated (cold) water vapor. Petuchowski & Bennett (1988) use the 10.3 GHz (2_{20}–2_{21}) HDO line to derive a value of $3 \times 10^{-9} < HDO/H_2 < 2 \times 10^{-8}$ in the Compact Ridge. Similar to Plambeck & Wright, they use previously derived water abundances to infer a large deuterium fractionation ($HDO/H_2O \approx 10^{-3}$). Hollis et al. (1986) use a tentative detection of H_3O^+ and a theoretical chemical model to infer $10^{-6} < H_2O/H_2 < 10^{-5}$, or 5–50 times our upper limit. Knacke et al. (1988) estimate $H_2O/CO \leq 0.01$–0.08 based on a 2–4 σ infrared absorption line (ν_3 1_{01}–2_{02} at 3801 cm^{-1}) toward the BN object. That is 3–25 times larger than our upper limit and 10–80 times our marginal detection.

In the Hot Core, observational estimates of H_2O/H_2 are from the 3_{13}–2_{20} observations of $H_2{}^{18}O$ by Jacq et al. (1988) and from observations of HDO. Assuming an LTE distribution of the 3_{13} and 2_{20} levels, Jacq et al. derive $H_2O/H_2 \sim 10^{-5}$. However, excitation uuncertainties are likely to limit the accuracy of the Jacq et al. results (cf. KK). HDO observations have been used by Moore et al. (1986) in the Hot Core to infer $H_2O/H_2 \leq 2 \times 10^{-5}$. Plambeck & Wright, who have less confidence in deuterium fractionation calculations use their much higher $X(HDO) \approx 10^{-7}$ to conclude that there is enhanced deuterium fractionation in the Hot Core, probably due to a recent sublimation of heavily fractionated water off of icy grains.

4.1.2. *The Orion Plateau*

The Orion Plateau is dense [$n(H_2) > 3 \times 10^6$ cm^{-3}] and compact (17″–30″), containing a high-velocity outflow, thought to be driven by IRc2 (see, e.g., Masson et al. 1984). The chemi-

TABLE 6

RESULTS

Source	T_{rms}[a] (K)	Min, Max V_{LSR} (km s^{-1})	Line Integral (K km s^{-1})	T_A^* Upper Limit (K)	H_2O/CO[b]
DR 21	2.3	−4.5, −0.5	-1.0 ± 3.6	2.5	<0.1
NGC 7538	2.3	−58.5, −53	12.6 ± 4.4	4.6	<0.03
W3	1.1	−46, −36	3.7 ± 2.2	0.9	<0.1
Orion A:					
Narrow features	0.9	6, 12	3.6 ± 1.6	1.15	<0.003
Plateau feature	0.9	−10, 30	6.4 ± 3.3	0.40	
NGC 2024	7.9	8.5, 12.5	14 ± 12	11	<0.003
Mon R2	7.7[c]	8.5, 12.5	-6 ± 12	7.5	<0.03
NGC 2264	1.3	6, 10	3.5 ± 2.1	2.1	<0.003
R UMa	3.8	...	...	...	...
Y UMa	3.2	...	...	...	...

[a] The rms noise is given for 1 MHz (0.54 km s^{-1}).
[b] Upper limits of T_A^* are compared to radiative transfer models using a $1/r^2$ density law.
[c] In Mon R2 only, noisy channels have been suppressed.

cal abundances in the high-velocity gas may therefore reflect the passage of a strong shock, though it is unsure how much of the gas has been so exposed. Evaporation of grain mantles could also raise the fractional water density. In any event, the predicted water abundance is much larger than in the preshock material, presumably typical of the Orion Ridge.

What sort of upper limit to the water abundance can be set from this single kinematic component? The Plateau is effectively a point source for our 2.'6 KAO beamwidth. Using $\Delta v = 40$ km s^{-1} (Masson et al. 1984; Kuiper, Zuckerman, & Rodriguez Kuiper 1981), we then get an upper limit of 0.4 K (Table 6). Assuming the source to be 20″ in diameter and diluted by the 2.'5 KAO beam, this implies an upper limit to the source brightness temperature of 22 K. The LVG model can then be used to yield a water abundance. From the 20″ source size, an assumed distance of 500 pc, and the velocity width of 40 km s^{-1}, we infer a velocity gradient of $dv/dr = 800$ km s^{-1} pc^{-1}. Taking $T_K = 180$ K and $n(H_2) = 5 \times 10^6$ cm^{-3}, we find $H_2O/CO < 0.22$, or $H_2O/H_2 < 1.5 \times 10^{-5}$.

This does not differ significantly from value of 1–20 $\times 10^{-6}$ reported by Phillips et al. (1980) based on observations of the 4_{14}–3_{21} line. However, our results are in direct conflict with an inferred water abundance in the Plateau Source by Olofsson (1984), who used observations of the 1_{10}–1_{11} line of HDO and a fractionation model to conclude that $H_2O/CO \approx 1$, or about 5 times our upper limit.

4.2. *NGC 2024*

NGC 2024 has been studied by Mundy et al. (1986) who have mapped $C^{34}S$ (5–4, 3–2, 2–1). When correlated with earlier $C^{32}S$ work, these maps show $n(H_2) = 10^{5.3}$ over a region larger than 8′ × 8′ and $n(H_2) = 10^6$–10^7 cm^{-3} in a small (1′–2′), core. Mezger et al. (1988) estimate from submillimeter continuum observations the presence of several small (0.01 pc) dense (10^8–10^9 cm^{-3}) condensations. Fitting these observations to an equivalent centrally dense core, we get $n = 2 \times 10^6$ cm^{-3} r^{-2} (arcmin), or about 10 times the density of the similar fit to the Orion A data. Assuming a kinetic temperature of 45 K, the $1/r^2$ model line emission is 12 K for an assumed H_2O/CO ratio of 0.003, or slightly larger than our upper limit of 11 K.

4.3. *NGC 2264*

Centered within the KAO beam is a site of intermediate-mass star formation. The IR source is cool compared to those in Orion A and in NGC 2024, and CS observations indicate $n(H_2) > 10^5$ (Schwartz et al. 1985). The kinetic temperature is 27 K, based on CO observations. The velocity of the CO source is 8 km s^{-1} with a velocity width of 3 km s^{-1}. There is also a 22 GHz water maser (30 Jy) within the KAO beam (15″ south) with components at 0, 5, and 18 km s^{-1}. The $H_2{}^{18}O$ spectrum has a noise level of 1.3 K. Over the velocity range of the ^{13}CO line (FWHM) this yields an upper limit of $T_A < 2.0$ K, with possible features ($\approx 3\ \sigma$) at both 5 and 9 km s^{-1}. For this source, we adopt a model of $n = 5 \times 10^5$ cm^{-3} r^{-2} (arcmin), intermediate between the Orion A and NGC 2024 models and derive from our upper limit a water abundance of $H_2O/CO \leq 0.003$.

4.4. *NGC 7538*

NGC 7538 is a site of massive star formation, well studied at infrared and millimeter wavelengths (Werner et al. 1979 and references therein; Pratap, Batrla, & Snyder 1990 and references therein). Within the KAO beam lie three infrared sources (IRS 1, 2, 3), the first of which is also a strong water maser (Genzel & Downes 1977). The distance to the source has been estimated to be 3.5 kpc (Israel, Habing, & de Jong 1973), the distance which we adopt in our calculations. Recent observations of HCN and HCO^+ by Pratap et al. (1990), using the BIMA interferometer show extensive structure including a high-velocity outflow, associated cavity, and a series (40–50) of dense [$n(H_2) > 10^5$ cm^{-3}] clumps with sizes ranging from 0.05 pc (the BIMA resolution limit) to 0.2 pc and having typical masses of 10–50 $M_\odot$. The temperature of the dense gas from observations of NH_3 is 170 K (Wilson et al. 1983) and 185 K from observations of HDO (Jacq et al. 1990). For our analysis, we use a kinetic temperature of 180 K and a distribution of densities characterized by $n = 5 \times 10^4$ cm^{-3} r^{-2} (arcmin). This is a distribution 40 times less dense than that for the NGC 2024 model, a difference primarily due to the larger distance of NGC 7538. The assumed velocity gradient is taken to be 1 km s^{-1} pc^{-1} based on a CO velocity width of 4 km s^{-1}. The resulting model line emission is 4.4 K for an assumed H_2O/CO ratio of 0.03, which is effectively the same as our 3 σ upper limit of 4.6 K.

4.5. *W3*

The W3 molecular core region has been extensively studied by Dickel et al. (1980), who have made maps using the $J = 1$–0 transitions of CO, ^{13}CO, and HCN and the $J = 2$–1 transition

of CS. These observations have been interpreted by Dickel (1980) in a model of the core region. The distance to the W3 core is taken to be 3 kpc, making it part of a giant cloud complex in the Perseus spiral arm (Wilson et al. 1974). The KAO beam contains the entire dense molecular core, with a density, $n(H_2)$, of 5×10^4 cm^{-3} in the central 1 pc (1.2 diameter) and in excess of 1×10^4 cm^{-3} within a diameter of 3.5 (Dickel 1980). Within the KAO beamwidth, we take the density to be 2×10^4 cm^{-3} and use a density model of $n = 3.5 \times 10^4$ cm^{-3} r^{-2}. The kinetic temperature is taken to be 35 K, the CO brightness temperature, though this is probably an underestimate near the embedded infrared source IRS 4. The assumed velocity gradient is taken to be 2 km s^{-1} pc^{-1} based on a CS velocity width of 5 km s^{-1} and an observed core region diameter of $\approx$2.5 pc (Dickel 1980). From the 0.9 K upper limit to the water emission, the derived water abundance is $H_2O/CO < 0.1$.

4.6. *DR 21*

The DR 21 region has been studied in detail by Richardson et al. (1986) using the $J = 2$–1 and 3–2 lines of CO, the $J = 4$–3 lines of HCN and HCO$^+$, and the $J = 7$–6 line of CS. Following the discussion of Richardson et al. (1986) we adopt a value of 47 K for the kinetic temperature and an average density $n(H_2)$ of 1×10^5 cm^{-3} in the central arcminute, with indications of denser clumps (10^6 cm^{-3}) having a filling factor of $\approx$0.1. These data fit well with a model having $n = 4 \times 10^4$ cm^{-3} r^{-2}, which is precisely the model adopted in an earlier observational study of DR 21 using the $J = 1$–0 transitions of CO and ^{13}CO (Dickel, Dickel, & Wilson 1978). We therefore adopt the same model and from our upper limit of 2.5 K derive $H_2O/CO < 0.1$.

4.7. *Mon R2*

The Mon R2 reflection association contains a massive (2×10^4 $M_\odot$) molecular cloud which has been studied in detail by Loren (1977) using various millimeterwave emission lines and with a spatial resolving power (2.6 at CO) almost identical to that of the KAO at 548 GHz. They report systematic motions, apparently systematic rotation and collapse, characterized by a spatial velocity gradient of 0.4 km s^{-1} pc^{-1} and a line-of-sight collapse velocity gradient which may be several times larger. The observed KAO position is in the direction of a deeply embedded infrared source as well as of the observed emission peaks of $J = 1$–0 CO, ^{13}CO, and HCO$^+$. The estimated kinematic distance is 850 pc (Racine 1968). Based on the strong HCO$^+$ emission within the central 3.0 we take the density to be greater than 1×10^5 cm^{-3}, yielding a density law of $n = 2 \times 10^5$ cm^{-3} r^{-2} (arcmin). The observed peak CO brightness is 28 K (Loren 1977), but the CO profile reflects heavy self-reversal and probably indicates a kinetic temperature about 40 K. Our observed upper limit is 7.5 K over the 8.5–12.5 km s^{-1} LSR velocity range which is the FWHM of Loren's $J = 1$–0 ^{13}CO line profile. We use $T_{kin} = 40$ K and a velocity gradient of 1.0 km s^{-1} pc^{-1} to yield an upper limit of $H_2O/CO < 0.03$.

4.8. *OH/IR Stars*

The two OH/IR stars, Y UMa and R UMa, are both late-type M giant stars. R UMa is an M3e–M9e long-period (302 day) Mira variable with prominent SiO and H_2O masers indicative of a dense wind. Y UMa is an M7 II semiregular variable with a shorter period (168 days) and no reported H_2O maser (cf. Benson et al. 1990 and references therein). In this paper, we do not analyze the stellar results, but report only the observational results. The analysis is quite different from that for the dense star-forming clouds in the sense that chemistry models must take account of the dominant role of neutral-neutral reactions close to the central star and of the important role of photodissociation. In addition, the line formation model must account for the strong infrared excitation, operating on vibration/rotation transitions and which will most likely dominate collisional rotational excitation.

5. DISCUSSION

5.1. *Interstellar Chemistry*

There are considerable uncertainties in predicting the water abundance in quiescent interstellar clouds. These uncertainties have two origins: (1) the destruction rate of water is set by the abundances of positive ions and of ionizing ultraviolent radiation, neither of which is well known and (2) there are several ways to initiate the incorporation of oxygen into molecular form, none of which is clearly the most attractive in normal, quiescent clouds.

The destruction processes of water set the overall time-scale for its chemical equilibrium:

$$t_d = [\Sigma k_i n(M_i)]^{-1} , \tag{10}$$

where the k_i are reaction rates with species M_i. In dense clouds, which are generally regarded as having high effective ultraviolet opacities, the leading gas-phase reactions (Mitchell et al. 1978) are with C$^+$ and HCO$^+$:

$$C^+ + H_2O \rightarrow HCO^+ + H \tag{11}$$

and

$$HCO^+ + H_2O \rightarrow H_3O^+ + CO , \tag{12}$$

with associated reaction rates listed in Table 7. However, reaction (12) may well lead straight back to water, depending on the branching ratio of the dissociative recombination reaction of H_3O^+ (see below). A major difference among model H_2O abundances can be related to their predicted abundances of C$^+$ (and HCO$^+$), which range over several orders of magnitude. The C$^+$ abundance is especially enhanced in regions of low opacity, where there is significant ultraviolet flux.

The total lifetime of water is set, not only by chemical reactions, but also by freezing onto grains and by direct photodissociation. The freezing rate is approximated as the grain collision rate:

$$k_{cond} = 1.53 \times 10^{-16} n(H_2)/\sqrt{M} \ (s^{-1}) , \tag{13}$$

where M is the molecular weight in atomic mass units (Herbst & Klemperer 1973). For $H_2{}^{18}O$, this yields 3.4×10^{-17} $n(H_2)$. Grain condensation may dominate the absolute fraction of water in dense clouds, but insofar as all species are similarly depleted, it is less likely to dominate relative abundances of H_2O/CO.

In addition, direct photodissociation can be significant, if there is a viable source of ionizing ultraviolet radiation. One possibility, explored by Sternberg, Dalgarno, & Lepp (1987), does not have any external UV radiation, but it does include UV radiation induced by cosmic rays, produced by secondary e^- excitation of H_2. They assume the canonical cosmic-ray

TABLE 7

MODEL ABUNDANCES

Model[a]	$n(H_2)$ $\times 10^4$ (cm^{-3})	T_K (K)	A_v	[O]/[C]	H_2O/CO	a_{17}[b] $\times 10^{-9}$ ($cm^3\ s^{-1}$)	a_{21}[b] $\times 10^{-7}$ ($cm^3\ s^{-1}$)	$[C^+]$ $\times 10^{-5}$ (cm^{-3})	$[HCO^+]$ $\times 10^{-6}$ (cm^{-3})	a_{11}[b] $\times 10^{-9}$ ($cm^3\ s^{-1}$)	a_{12}[b] $\times 10^{-9}$ ($cm^3\ s^{-1}$)	t_d $\times 10^4$ (yr)
Opaque Clouds, Normal Abundances												
LHH1	1	10	∞[c]	2.4	0.062	2.0	6.5	0.7	3.1	2.0	0.5	203
P + H3	2	50	∞	2.4	0.055	0.8	6.5	1.3	7.1	2.7	2.7	58
GLF3-L	1	10	∞	2.4	0.051	0.8	55	2.0	84	2.7	0.0	59
MGK3	50	50	∞	2.4	0.048	0.4	10	2.5	141	2.0	1.0	22
GLF4-L	10	10	∞	2.4	0.044	0.8	55	1.8	280	2.7	0.0	65
GLF2	10	10	∞	2.4	0.043	0.8	55	3.8	7.3	2.7	0.0	31
LHH2	10	10	∞	2.4	0.040	2.0	6.5	0.6	14	2.0	0.5	167
P + H4	40	50	∞	2.4	0.035	0.8	6.5	1.0	35	2.7	2.7	26
BR2H	1	30	∞	2.4	0.032	0.8	3.5	2.5	...	2.6	2.5	<49
H + L2	1	10	5	2.4	0.031	2.0	6.5	6	69	2.0	0.5	21
BR1H	10	70	∞	2.4	0.025	0.8	3.5	...	50	2.6	2.5	<25
H + L1	1	10	500	2.4	0.024	2.0	6.5	1.1	100	2.0	0.5	44
VIA1-L	0.5	10	11	3.1	0.018	0.8	130	0.4	70	2.7	3.2	13
VIA1-H	0.5	10	11	3.1	0.017	0.8	130	0.2	2.8	2.7	3.2	220
BR2L	1	30	∞	2.4	0.016	0.8	3.5	2.5	...	2.6	2.5	<51
VIA2-H	5	10	11	3.1	0.015	0.8	130	0.2	7.7	2.7	3.2	105
H + L3	1	50	20	2.4	0.014	2.0	6.5	1.1	240	2.0	0.5	22
SDL-L	1	50	[d]	2.4	0.007[e]	0.8	100	6.5	...	7.5	3.2	<6.5
GLF1	1	10	∞	2.4	0.0069	0.8	55	36	0.12	2.7	0.0	3.2
BR1-L	10	70	∞	2.4	0.0063	0.8	3.5	...	1000	2.6	2.5	<1.6
Carbon-rich Models												
H + K1	1	30	∞	1.17	0.00053	2.0	6.5	80	100	2.0	0.5	1.9
H + L4	1	10	500	0.78	0.00015	2.0	6.5	41	73	2.0	0.5	3.7
Low-Opacity (Photoionized) Regions												
P + H2	0.25	22	1	2.4	0.00001	0.8	6.5	29,000	0.02	2.7	2.7	0.004

[a] Key to model codes: H + K: Herbst & Klemperer 1973; BR Brown & Rice 1986; LHH: Leung, Herbst, & Huebner 1984, "normal" metallicity models; H + L: Herbst & Leung 1986; GLF: Graedel, Langer, & Frerking 1982; P + H: Prasad & Huntress 1980; MGK: Mitchell, Ginsburg, & Kuntz 1978; SDL: Sternberg, Dalgarno & Lepp 1987; VIA: Viala 1986 (L = low metal models; H = high or normal metallicity models).

[b] a_{17}, a_{21}, a_{11}, and a_{12} are the rate constants used by the various models for reactions (17), (21), (11), and (12) in the text.

[c] A value of ∞ means that photodissociation reactions were not included at all.

[d] The model of Sternberg, Dalgarno, & Lepp 1987 does not have any external UV radiation, but it does include UV radiation induced by cosmic rays, produced by secondary e^- excitation of H_2. They assume the canonical cosmic-ray ionization rate of $\xi = 10^{-17}\ s^{-1}$. The resulting photodissociation rate of water is $7.69 \times 10^{-15}\ s^{-1}$, which is not significant relative to the ordinary chemical destruction rates.

[e] Assuming $X(CO) = 10^{-4}$. The authors give only $X(H_2O)$.

ionization rate of $\xi = 10^{-17}\ s^{-1}$. The resulting photodissociation rate of water is

$$k_{CR} = 7.69 \times 10^{-15}\ s^{-1}\ .$$

Also uncertain are the initial steps leading to the formation of water. These steps are difficult in cool gas, easier in warm gas, and very easy in strongly shocked material. Because internal shocks and warm, interclump gas are thought to exist in large molecular clouds, the origins of water can be in doubt.

In cool interstellar gas, the chemistry of oxygen is thought (cf. Herbst & Klemperer 1973) to start with a series of ion-molecule reactions involving atomic oxygen and the rather rare molecular ion H_3^+, a by-product of cosmic ray ionization:

$$H_2 + \text{cosmic ray} \rightarrow H_2^+ + e^- \quad (14)$$

or

$$\rightarrow H^+ + H + e^- \quad (15)$$

followed by

$$H_2^+ + H_2 \rightarrow H_3^+ + H \quad (16)$$

and

$$H_3^+ + O \rightarrow H_2 + OH^+\ . \quad (17)$$

Model abundances depend on the assumed rates of process (17), and these are listed in Table 7.

The space density of H_3^+ is usually taken to be about 10^{-5} cm^{-3}, and more or less invariant with cloud density over a range of 10^4–10^7 cm^{-3} because the formation process per unit volume is linear with density and the destruction processes (reactions with other molecules and recombination) vary as the density squared. Recent laboratory measurements have affected the perceived recombination rate of H_3^+ (Adams & Smith 1987; Amano 1988) but probably do not profoundly affect the chemistry of water (Viala 1986). There have been quite a number of comprehensive chemistry models which predict the water abundance in dense, warm gas, and some of these are listed in Table 7. As can be seen, these models yield differing values of $[H_2O]/[CO]$. Some of these differences can be attributed to their adopted reaction rates and gas-phase elemental abundances.

In the last column of Table 7 is listed the water lifetime for each model, as calculated from equation (10). As can be seen, the models with the lowest predicted water abundances are those which, for one reason or another, have the largest destruction rates. The six models yielding $H_2O/CO < 0.01$ are precisely those with predicted water lifetimes of less than 10^5

yr. In the models of opaque clouds with normal elemental abundances, the three smallest model abundances are from the models: SDL-L, GLF1, and BR1-L. These three models, respectively, use large reaction rates for the reaction (11) with C^+ (SDL-L), have a large C^+ abundance (GLF1), and have a large HCO^+ abundance (BR1-L). The carbon-rich and the photoionized models (H + K1, H + L4, P + H2) also have very short lifetimes due to their large C^+ abundances. Thus we see the importance of the destruction reactions in setting the predicted water abundance.

In warmer regions (> 50 K), the endothermic reaction

$$H^+ + O \rightarrow H + O^+ - k \times 232 \text{ K} \quad (18)$$

followed by

$$O^+ + H_2 \rightarrow OH^+ + H$$

may provide a more rapid entry into subsequent oxygen chemistry. Below 50 K, reaction (18) is not significant since the rate constant decreases from 10^{-11} cm^3 s^{-1} to 10^{-19} cm^3 s^{-1} over the temperature drop from 50 to 10 K (Field & Steigman 1971).

In either case, OH^+ is rapidly converted into H_3O^+ by ion-molecule reactions with molecular hydrogen:

$$OH^+ + H_2 \rightarrow OH_2^+ + H \quad (19)$$

and

$$OH_2^+ + H_2 \rightarrow H_3O^+ + H . \quad (20)$$

The formation of neutral water is then by a dissociative recombination reaction:

$$H_3O^+ + e^- \rightarrow H_2O + H . \quad (21)$$

Doubt exists about the rate of reaction (21) in part due to an uncertain branching ratio with a major competing channel:

$$H_3O^+ + e^- \rightarrow OH + H_2 \text{ (or H + H)} . \quad (22)$$

The fraction of recombinations leading to the formation of water (21) has been variously taken as 50% (Herbst & Klemperer 1973), 20% (Herbst 1978), 33% (Viala 1986) and $\approx$100% (Bates 1986; Lepp & Dalgarno 1987). Recently, a measurement of the channel leading to the production of OH (reaction 22) has been made by Herd, Adams, & Smith (1990) leading to an estimate of its efficiency of 65% $\pm$ 15%. Assuming that the remaining reactions lead to the production of water (as opposed to atomic oxygen), the branching ratio for water is 35% $\pm$ 15%, very close to the value used by Viala. In addition to uncertainty about the branching ratio, the total reaction cross-section varies considerably from model to model (Table 7).

In regions which have experienced strong shocks (> 7 km s^{-1}), oxygen chemistry may proceed rather more readily by means of neutral, endothermic reactions, either from atomic or molecular oxygen. For example,

$$H_2 + O \rightarrow OH + H \quad (23)$$

or

$$H + O_2 \rightarrow OH + O \quad (24)$$

followed by

$$H_2 + OH \rightarrow H_2O + H . \quad (25)$$

The gas fraction of CO is constant throughout the shock so long as the shock velocity does not exceed the dissociation limit for H_2 (11 km s^{-1}). In a model of a 10 km s^{-1} shock propagating into a gas of 30 K and $n(H_2) = 10^4$ cm^{-3}, Iglesias & Silk (1978) find that most oxygen not bound up in CO ends up as water. This result is in essential agreement with more recent models by Graff & Dalgarno (1987) and Leen & Graff (1988) of a 10 km s^{-1} shock propagating into a medium of $n(H_2) = 10^5$ cm^{-3}. Therefore, depending on the initial fraction of oxygen tied up in gas-phase CO, the postshock H_2O/CO ratio can vary from 0.5 to 1.5. A high water abundance might then persist for up to 10^5 yr (col. [13], Table 7) in the postshock gas, depending on the density of the destructive ions C^+ and HCO^+.

5.2. *The Physical Models of Dense Clouds*

In § 5.1, we have examined the chemistry issues which affect the water abundance, and we find that the measured H_2O/CO upper limits fall below those generally predicted for dense, warm molecular gas in dark cloud interiors. Here, we examine the implications in terms of physical modeling. In Table 7, we see that the water abundance is sensitive to destruction processes, including reactions with C^+ (reaction [11]) and HCO^+ (reaction [12]) and by freezing onto icy grains. Even in the case of the carbon-rich models, with [O]/[C] set to 0.78 (H + L4) or 1.17 (H + K1), the reduction of water is effectively driven by an excess of C^+ rather than by the absence of available oxygen to make water. Is such a decrease in the oxygen abundance plausible? It is difficult to believe that such a decrease can result from an overall reduction in the total (gas and grains) local abundance of oxygen. It is not expected on the basis of abundances either in stars or in the diffuse interstellar medium (e.g., Morton 1975). Depletion onto grains is a possibility, but the only form which could seriously deplete oxygen is water itself, in the form of icy mantles. At present, the observational evidence for icy grains in dense clouds can neither substantiate nor rule out such a possibility. However, the expectation is that the temperature boundary where icy mantles can either grow or shrink falls in the region of 50–100 K, or very close to the gas kinetic temperatures of the molecular clouds listed in Table 6 (cf. Gordon 1988).

The destruction rate of water might be increased by increasing the photoionization rate or by increasing C^+ (or, possibly, HCO^+). In practice, an increase of C^+ likewise implies more ultraviolet radiation. An increase in the assumed HCO^+ abundance seems to be in conflict with observations. The observations of HCO^+ in OMC-1 yield $N(HCO^+) = 1.3 \times 10^{15}$ cm^{-2} or a space density of 4.3×10^{-4} cm^{-3} assuming a uniform distribution over 1 pc (Leung et al. 1984). This value is larger than some, but not all, of the model HCO^+ abundances in Table 7 and by itself would not explain our low limit to the water abundance. Results in other dense clouds are similar. There are, however, no reliable observations of the C^+ abundances, and there are, indeed, other independent suggestions that it might be higher than is often supposed. Destruction of water by reaction (11) implies a significant concentration of ionized carbon, expected to be a common constituent at the surface layers of clouds, but not in their interiors. This lack can be overcome if there is adequate ionizing UV radiation in the dark cores of clouds.

Independent observational support comes in the form of C^0 observations. C^0, like C^+, is found primarily in regions of modest ($A_v < 2$) opacity (Fig. 7). Estimates for the C^0 abundance are based on recent observations of 809 GHz C^0 (Zmuidzinas, Betz, & Goldhaber 1986; Jaffe et al. 1985) in

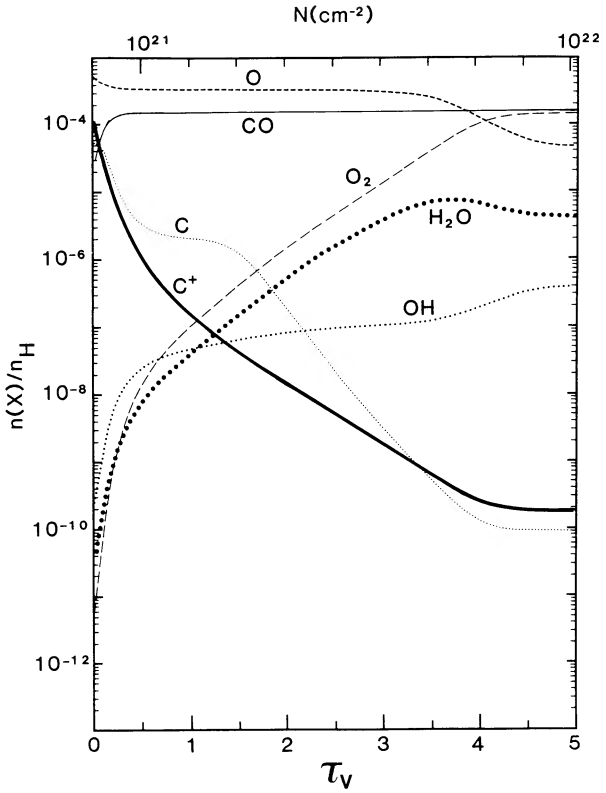

FIG. 7.—This figure, from Viala (1986), shows the dependence of various species on the cloud opacity. H_2O exists primarily in dark interiors ($A_v > 3$) while CO persists out to very small opacities ($A_v = 0.2$). C^0 and C^+ both exist primarily at modest opacities ($A_v < 3$). Our low observed water abundances and the large observed C^0 abundances in giant clouds together suggest the presence deep in cloud interiors of ionizing radiation.

combination with earlier results of 492 GHz C^0 (Phillips & Huggins 1981). Together, they yield $C^0/CO = 0.04$ in the Orion Ridge and $C^0/CO \sim 0.1$ in five dense clouds. The derived C^0 excitation temperatures of 30–60 K are typical of temperatures of the cloud interiors. A C^0/CO value of 0.1 is about 5 times larger than typical model predictions (Viala 1986) and suggests the presence of increased C^+ as well.

C^+ is sensitive to the presence of ionizing radiation and is not generally thought to be produced in the interiors of giant clouds such as OMC-1. However, it may be that excess C^+ results from density inhomogeneities which seem to be present in GMCs (cf. Keene et al. 1985). Several authors have analyzed the structures of dense clouds and have concluded that evidence for such density structure does exist over many distance scales (Perault, Falgarone, & Puget 1986). The implications of clumping on the penetration of ionizing radiation has been recently examined by Boissé (1990), who has performed analytical and Monte Carlo simulations of a medium containing dense clumps. He concludes that in some circumstances clumping can enhance the interior UV radiation by one or two orders of magnitude over that expected in a uniform cloud. Supporting observational evidence comes from the observed distribution of C^+ in M17 (Stutzki et al. 1988).

6. CONCLUSIONS

1. The half-millimeter wavelength ground-state transition of ^{18}O water has been observed in seven GMCs with essentially negative results or with possible, marginal detections (~ 2–$3\ \sigma$) in three sources.

2. When the results are modeled using an LVG code and a density model of the cloud cores, upper limits to the H_2O/CO fractional abundance can be made. In three sources we find $H_2O/CO < 0.003$, and in the four other sources the limits are less sensitive. The limits are derived on the basis of radiative transfer model incorporating LVG analysis for the low-opacity cloud exterior.

3. The upper limits are significantly smaller than suggested water abundances based on HDO observations. The HDO results may be too difficult to interpret in terms of a water abundance, due to an unknown degree of deuterium fractionation.

4. The upper limits are less than estimates based on observations of lines originating from levels which are very high on the rotational ladder of water. These high-excitation lines may be too difficult to interpret due to nonthermal excitation.

5. The upper limits are less than abundances predicted by many chemistry models. This lack may result from the formation of icy grains or from the chemical destruction of water by ionizing radiation. Such destruction might occur as a result of cloud fragmentation, offering enhanced entry of interstellar UV and a high abundance of C^+. Such a model needs better definition for the case of GMCs.

6. A possibility which should be checked by improved models and observations is that the cloud exterior effectively diffuses the emergent 548 GHz radiation.

It is a pleasure to acknowledge scientific contributions from several colleagues, including J.-L. Puget, A. Wootten, M. Perault, P. Boissé, Y. P. Viala, and B.-G. Andersson. We are especially grateful to P. Batelaan, M. Schaefer, L. Denis, C. Rosolen, and P. Dierich for much of the engineering support which made this work possible. We acknowledge the very hard and thorough work put in by an anonymous referee. Though we could not agree on all points, we do wish that all papers could undergo such intense scrutiny. We also acknowledge the total support of the KAO staff and especially to J. McClanahan who acted as ombudsman for our 1987 program. The research described in this paper was carried out by the Jet Propulsion Laboratory, California Institute of Technology under contract to the National Aeronautics and Space Administration. One of us (P. W.) would like to acknowledge the hospitality offered to him at the Ecole Normale Superieure during his stay there in 1987 June. Another one of us (L. P.) would like to acknowledge the hospitality offered to him at J.P.L. during 1988 July and August.

REFERENCES

Adams, N. G., & Smith, D. 1987, in IAU Symposium 120, Astrochemistry, ed. M. S. Vardya & S. P. Tarafdar (Dordrecht: Reidel), 1
Amano, T. 1988, ApJ, 329 L121
Bates, D. R. 1986, ApJ, 306, L45
Benson, P. J., Little-Marenin, I. R., Woods, T. C., Attridge, J. M., Blais, K. A., Rudolph, D. B., Rubiera, M. E., & Keefe, H. L. 1990, ApJS, 74, 911
Blake, G. A., Sutton, E. C., Masson, C. R., & Phillips, T. G. 1987, ApJ, 315, 621
Boissé, P. 1990, A&A, 228, 483
Brown, R. D., & Rice, E. H. N. 1986, MNRAS, 223, 405
Cernicharo, J., Thum, C., Hein, H., John, D., Garcia, P., & Mattioco, F. 1990, A&A, submitted
Clough, S. A., Beers, Y., Klein, G. P., & Rothman, L. S. 1973, J. Chem. Phys., 59, 2254
De Lucia, F. C., Helminger, P., & Kirchhoff, W. H. 1974, J. Phys. Chem. Ref. Data, 3, 211
Dickel, H. R. 1980, ApJ, 238, 829

Dickel, H. R., Dickel, J. R., Wilson, W. J., & Werner, M. W. 1980, ApJ, 237, 711
Dickel, J. R., Dickel, H. R., & Wilson, W. J. 1978, ApJ, 223, 840
Dyke, T. R., & Muenter, J. S. 1973, J. Chem. Phys., 59, 3125
Erickson, N. R., & Plambeck, R. L. 1987, private communication
Field, G. B., & Steigman, G. 1971, ApJ, 166, 59
Genzel, R., & Downes, D., 1977, A&AS, 30, 145
Goldreich, P., & Kwan, J. 1974, ApJ, 189, 441
Goldsmith, P. F., Langer, W. D., Schloerb, P., & Scoville, N. Z. 1980, ApJ, 240, 524
Gordon, M. A. 1988, ApJ, 331, 509
Graedel, T. E., Langer, W. D., & Frerking, M. A. 1982, ApJS, 48, 321
Graff, M. M., & Dalgarno, A. 1987, ApJ, 317, 432
Green, S. 1980, ApJS, 42, 103
Green, S., & Thaddeus, P. 1976, ApJ, 205, 766
Hartquist, T. W., Oppenheimer, M., & Dalgarno, A. 1980, ApJ, 236, 182
Herbst, E. 1978, ApJ, 222, 508
Herbst, E., & Klemperer, W. 1973, ApJ, 185, 505
Herbst, E., & Leung, C. M. 1986, MNRAS, 222, 689
Herd, C. R., Adams, N. G., & Smith, D. 1990, ApJ, 349, 388
Hollis, J. M., Churchwell, E. B., Herbst, E., & De Lucia, F. C. 1986, Nature, 322, 524
Iglesias, R. R., & Silk, J. 1978, ApJ, 226, 851
Israel, F. P., Habing, H. J., & de Jong, T. 1973, A&A, 27, 143
Jacq, T., Jewell, P. R., Henkel, C., Walmsley, C. M., & Baudry, A. 1988, A&A, 199, L5
Jacq, T., Walmsley, C. M., Henkel, C., Baudry, A., Mauersberger, R., & Jewell, P. R. 1990, A&A, 228, 447
Jaffe, D. T., Harris, A. I., Silber, M., Genzel, R., & Betz, A. L. 1985, ApJ, 290, L59
Keene, J., Blake, G. A., Phillips, T. G., Huggins, P. J., & Beichman, C. A. 1985, ApJ, 299, 967
Knacke, R. F., Larson, H. P., & Noll, K. S. 1988, ApJ, 335, L27
Kuiper, T. B. H., Swanson, P. N., Dickinson, D. F., Rodriguez, Kuiper, E. N., & Zimmermann, P. 1984, ApJ, 286, 310 (KK)
Kuiper, T. B. H., Zuckerman, B., & Rodriguez-Kuiper, E. N. 1981, ApJ, 251, 88
Leen, T. M., & Graff, M. M. 1988, ApJ, 325, 411
Lepp, B., & Dalgarno, A. 1987, BAAS, 18, 1029
Leung, C. M., Herbst, E., & Huebner, W. F. 1984, ApJS, 56, 231
Loren, R. B. 1977, ApJ, 215, 129
Masson, C. R., et al. 1984, ApJ, 283, L37
Menten, K. M., Melnick, G. J., & Phillips, T. G. 1990, ApJ, 350, L41
Mezger, P. G., Chini, R., Kreysa, E., & Wink, J., E., & Salter, C. G. 1988, A&A, 191, 44
Mitchell, G. F., Ginsburg, J. L., & Kuntz, P. J. 1978, ApJS, 38, 39
Moore, E. L., Langer, W. D., & Huguenin, G. R. 1986, ApJ, 306, 682
Morton, D. C. 1975, ApJ, 197, 85
Mundy, L. G., Snell, R., Evans, N. J., Goldsmith, P. F., & Bally, J. 1986, ApJ, 306, 670
Olofsson, H. 1984, A&A, 134, 36
Palma, A., Green, S., DeFrees, D. J., & McLean, A. D. 1988, ApJS, 68, 287
———. 1989, ApJS, 70, 681
Penzias, A. A. 1975, in Atomic and Molecular Physics and the Interstellar Matter, ed. R. Balian, P. Encrenaz, & J. Lequeux (Amsterdam: North-Holland), 373
Perault, M., Falgarone, E., & Puget, J.-L. 1986, A&A, 157, 139
Petuchowski, S. J., & Bennett, C. L. 1988, ApJ, 326, 376
Phillips, T. G., & Huggins, P. J. 1981, ApJ, 251, 533
Phillips, T. G., Jefferts, K. B., & Wannier, P. G. 1973, Ap. Letters, 15, 17
Phillips, T. G., Kwan, J., & Huggins, P. J. 1980, in IAU Symposium 87, Interstellar Molecules, ed. B. H. Andrew (Dordrecht: Reidel), 21
Phillips, T. G., Scoville, N. Z., Kwan, J., Huggins, P. J., & Wannier, P. G. 1978, 222 L59
Plambeck, R. L., & Wright, M. H. C. 1987, ApJ, 317, L101
Prasad, S. S., & Huntress, W. T., Jr. 1980, ApJS, 43, 1
Pratap, P., Batrla, W., & Snyder, L. E. 1990, ApJ, 351, 530
Racine, R. 1968, AJ, 73, 233
Richardson, K. J., White, G. J., Phillips, J. P., & Avery, L. W. 1986, MNRAS, 219, 167
Schwartz, P. R., Thronson, H. A., Jr., Odenwald, S. F., Glaccum, W., Loewenstein, R. F., & Wolf, G. 1985, ApJ, 292, 231
Scoville, N. Z., & Solomon, P. M. 1974, ApJ, 187, L67
Sternberg, A., Dalgarno, A., & Lepp, S. 1987, ApJ, 320, 676
Stutzki, J., Stacey, G. J., Genzel, R., Harris, A. I., Jaffe, D. T., & Lugten, J. B. 1988, ApJ, 332, 379
Taylor, J. A., Tannenwald, P. E., Erickson, N. R., Dionne, G. F., & Fitzgerald, J. F. 1985, Internat. J. Infrared Millimeter Waves, 6, 687
Viala, Y. P. 1986, A&AS, 64, 391
Wannier, P. G. 1980, ARA&A, 18, 399
Waters, J. W., et al. 1980, ApJ, 235, 57
Werner, M. W., Becklin, E. E., Gatley, I., Matthews, K., & Wynn-Williams, C. G. 1979, MNRAS, 188, 463
Wilson, T. L., Mauersberger, R., Walmsley, C. M., & Batrla, W. 1983, A&A, 127, L19
Wilson, W. J., Schwartz, P. R., Epstein, E. E., Johnson, W. A., Etcheverry, R. D., Mori, T. T., Berry, G. G., & Dyson, H. B. 1974, ApJ, 191, 357
Wootten, A., Boulanger, F., Bogey, M., Combes, F., Encrenaz, P. J., Gerin, M., & Ziurys, L. 1986, A&A, 166, L15
Zmuidzinas, J., Betz, A. L., & Goldhaber, D. M. 1986, ApJ, 307, L75